

## Emergence of Synchronization in a Driven-Dissipative Hot Rydberg Vapor

Karen Wadenpfehl<sup>1,2,\*</sup> and C. Stuart Adams<sup>1,†</sup>

<sup>1</sup>Joint Quantum Centre (JQC) Durham-Newcastle, Department of Physics, Durham University, Durham, DH1 3LE, United Kingdom  
<sup>2</sup>Physikalisches Institut, Universität Heidelberg, Im Neuenheimer Feld 226, 69120 Heidelberg, Germany



(Received 9 June 2023; accepted 23 August 2023; published 6 October 2023)

We observe synchronization in a thermal (35–60 °C) atomic (Rb) ensemble driven to a highly excited Rydberg state (principle quantum number  $n$  ranging from 43 to 79). Synchronization in this system is unexpected due to the atomic motion; however, we show theoretically that sufficiently strong interactions via a global Rydberg density mean field cause frequency and phase entrainment. The emergent oscillations in the vapor's bulk quantities are detected in the transmission of the probe laser for a two-photon excitation scheme.

DOI: 10.1103/PhysRevLett.131.143002

Nonlinear systems are abundant in nature, where the nonlinearities introduce a range of rich and varied phenomena. Well known is the ability of nonlinear systems to generate multiple steady states, so that the system's state is determined by its past trajectory and hysteresis loops may form. Such multistable states have been observed numerously in biological [1–4], mechanical [5–7], and atomic systems [8–11]. Nonlinear dynamics and bifurcation theory provide a modeling framework of these phenomena, enabling a fundamental understanding of the underlying processes from within a generalized mathematical framework.

When adding dissipation to a conservative nonlinear system, the resulting dynamics get even richer, and the system can support rather unexpected types of stable solutions. Under certain conditions, dissipative systems with nonlinearities can support chaotic behavior [12,13] or limit cycles and time-periodic solutions [14,15]. A Hopf bifurcation may cause the appearance of attractive limit cycles, which leads to self-sustained oscillations of the system. This oscillatory behavior is not imprinted by an external drive but arises fundamentally from the system's dynamics. Such self-oscillating systems have been found to model biological processes [16–20] and physical systems [21–24].

A very curious question regards the behavior of an ensemble of self-sustained oscillators experiencing a form of coupling to another, or to an external force. First studied by Kuramoto for an ensemble of globally coupled oscillators with different natural frequencies [25], it has been found that—under certain conditions—all or a subset of the oscillators begin to lock in frequency and phase [26–28].

As a result, a transition toward a synchronized state occurs in the ensemble. This synchronization transition has been used to explain, e.g., the strong lateral vibrations of the Millennium bridge, London, on its opening day [29], though this is contested [30], or the Belousov-Zhabotinsky and other chemical reactions [31,32]. In nature, synchronization occurs in ensembles of fireflies flashing in unison [33], the chirps of snowy tree crickets [34], and occasionally in the applause of audiences [35].

To further study the emergence of synchronization and the resulting nonequilibrium dynamics, a simple and easily controllable system with a macroscopic number of coupled oscillators and tunable properties is highly desirable. In the following, we demonstrate that the occurrence of a synchronized phase is expected in a continuously driven, dissipative three-level system with a power-law coupling to a mean field, and report on the observation of synchronization in a hot Rydberg vapor. A surprising, but expected, feature of this system is that oscillations of the bulk quantities remain observable even though the individual constituents are undergoing random motion.

Rydberg atoms are known to interact strongly with a power-law scaling in distance. This translates into a mean-field approach [36] with power-law scaling  $\beta$  of the Rydberg level shift in Rydberg density  $\rho_{rr}$ . A similar power-law scaling also can be used to model the level shift induced by ionization [37] or other mean-field inducing mechanisms. Adopting this mean-field approach, the resulting equations of motion (EOMs) are formulated for a three-level basis set with coherent driving by  $\Omega_x$  and dissipation  $\Gamma_{yz}$ ; see Fig. 1(a). For  $\beta \neq 0$ , the EOMs are nonlinear, and their steady states are defined by the roots of a polynomial of order  $\max(4\beta + 1, 1)$  in  $\rho_{er}^i$ .

The resulting steady-state solutions of the nonlinear EOMs reveal regions of multistability where an odd number of equilibria exist for one set of parameters  $\Omega_x, \Delta_x, \Gamma_{yz}, V, \beta$ . To extract the stability of the solutions, the spectrum of

Published by the American Physical Society under the terms of the Creative Commons Attribution 4.0 International license. Further distribution of this work must maintain attribution to the author(s) and the published article's title, journal citation, and DOI.

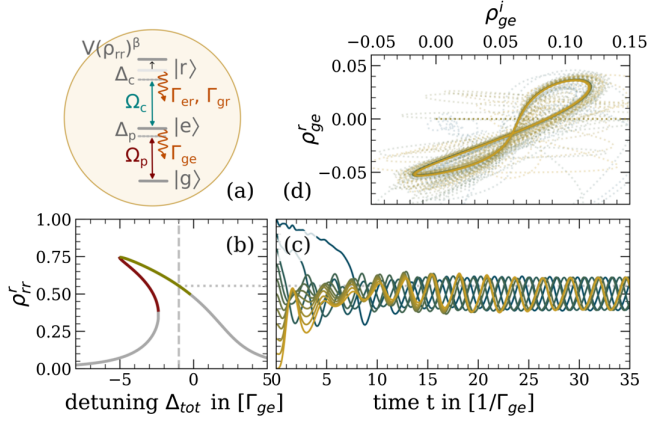


FIG. 1. Single velocity class model. The basic model with the relevant parameters is shown in (a). An example steady-state solution of the resulting nonlinear OBEs is shown in (b) where the dark-red steady-state branch is repulsive and green indicates the limit cycle region. For a fixed detuning  $\Delta_c/\Gamma_{ge} = -1$ , indicated by the dashed line, the time evolution from an initial state  $|\Psi\rangle_{t=0} = (1-x)|g\rangle + x|r\rangle$  with  $x \in [0, 1]$  toward a limit cycle is shown in (c). For the same time traces, a phase space projection of the limit cycle in the  $\rho_{ge}$ -plane is shown in (d). The other model parameters were set to  $\Delta_p = 0$ ,  $\Omega_p/\Gamma_{ge} = 3.8$ ,  $\Omega_c/\Gamma_{ge} = 2$ ,  $V/\Gamma_{ge} = -12$ ,  $\Gamma_{er}/\Gamma_{ge} = 10^{-5}$ ,  $\Gamma_{gr}/\Gamma_{ge} = 10^{-2}$ , and  $\beta = 3$ .

eigenvalues  $\lambda_j$  of the linearization (Jacobi) is evaluated at the steady state [38]. Stability is guaranteed if  $\text{Re}(\lambda_j) < 0$  for the eight nonconstant eigenvalues. Consequently, the repulsive branch marked in red in Fig. 1(b) is detected by spectral analysis. However, the steady states indicated in green are also unstable. Here, a Hopf bifurcation occurs where a complex-conjugate pair of eigenvalues  $\lambda_j$  crosses the imaginary axis and renders the steady state unstable. As a result, the system is attracted toward a limit cycle which leads to robust self-sustained oscillations of the system parameters in time. Figures 1(c) and 1(d) show that the system is attracted to the same limit cycle for different initial states, but each initial state leads to a different phase in the limit cycle at any fixed time  $t$ . This freedom of phase in the limit cycle is indicative of a self-oscillating system and fundamentally distinguishes it from a periodically driven system where the phase in the limit cycle is locked to that of the drive. The freedom of phase in the resulting limit cycle has also been described using the language of continuous time crystals [39,40]. The time-crystal interpretation in the context of our experiment is discussed in Appendix E of the Supplemental Material [41].

Although optical bistability has been found experimentally in driven-dissipative hot Rydberg vapors [10], one would intuitively expect any oscillations in this system to average out due to atomic motion. The motion-induced dephasing for different atomic velocities results in a spread of the natural frequencies of the limit cycles and the phases therein. Although about half of the velocity classes are attracted toward a limit cycle, no macroscopic oscillations can be seen, as shown by the black line in Fig. 2(a).

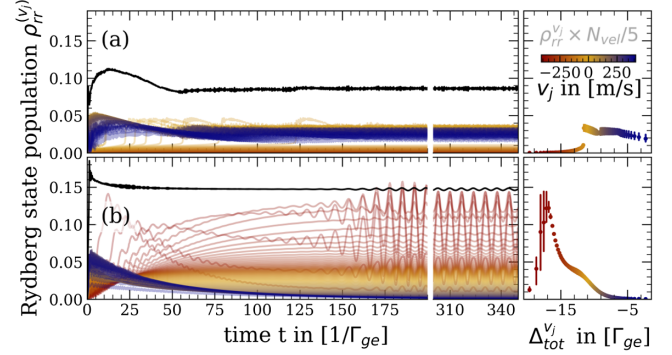


FIG. 2. Thermal vapor simulation showing emergence of synchronization. A thermal vapor simulation for uncoupled (a) and coupled (b) velocity classes shows the emergence of synchronization via the Rydberg density induced mean field. The time evolution and corresponding steady-state spectrum are shown on the left and right, respectively. Simulation parameters were  $\Omega_p/\Gamma_{ge} = 6$ ,  $\Omega_c/\Gamma_{ge} = 4$ ,  $\Delta_p = 0$ ,  $\Delta_c/\Gamma_{ge} = -11$ ,  $\Gamma_{er}/\Gamma_{ge} = 10^{-5}$ ,  $\Gamma_{gr}/\Gamma_{ge} = 10^{-2}$ ,  $V/\Gamma_{ge} = -800$ ,  $\beta = 2$  and  $N_{\text{vel}} = 101$  velocity classes with equal populations. The atomic velocity distribution corresponds to that of a rubidium vapor on the  $D_2$  line at 48 °C.

However, the above argumentation does not account for the spatial dimension of the situation. The Rydberg level shift of any atom in the vapor depends on the spatial Rydberg density of its local environment so that the different velocity classes do not evolve independent of another. Rydberg atoms of one velocity class experience a level shift depending on the Rydberg population of the other velocity classes in the vapor and, in turn, influence the dynamics of these other velocity classes. When taking this global coupling between the velocity classes into account, the resulting dynamics of the vapor is very different as shown in Fig. 2(b) (see also Appendix C in the Supplemental Material [41]). After an initial transient phase, synchronization sets in where the velocity classes begin to oscillate in lockstep with a single frequency and fixed phase relation. This is possible because the phase of a velocity class within its limit cycle is free and therefore easily adjusted by the mean field. With a growing number of velocity classes oscillating in phase lock, the mean field strength increases which forces even more velocity classes to align their oscillations until eventually a partially or completely synchronized state is reached.

This transition toward a synchronized state of globally coupled oscillators is known since Christiaan Huygens's time [45] and has since been studied extensively from a mathematical perspective. After the initial work by Winfree [46] and Kuramoto [25], the study of synchronization has been extended to more general forms of the global coupling force [27,28] and other situations [47]. Famous examples where synchronization is experimentally demonstrated for few oscillators is the synchronization of pendulum clocks [45] or metronomes [48] fixed to a common support which

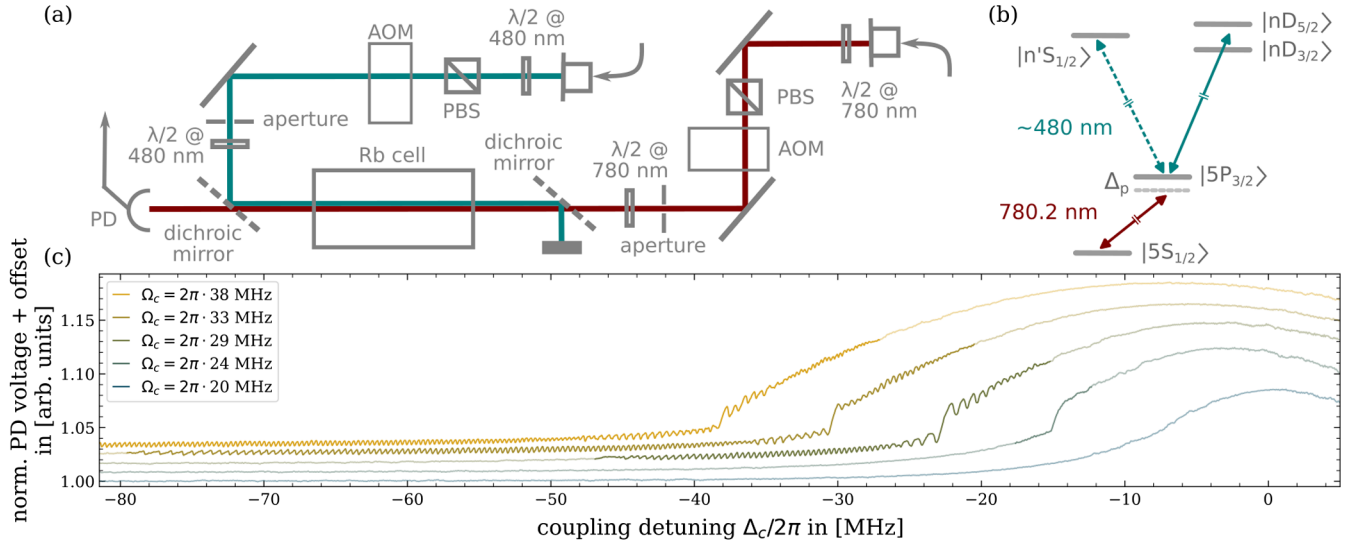


FIG. 3. Setup and example onset of oscillations. (a) The counterpropagating probe and coupling lasers are polarization cleaned with a polarizing beamsplitter (PBS) after exiting the fibers. The subsequent acousto-optic modulator (AOM) and aperture are used to remote control the laser powers incident on the heated, 4 cm long rubidium cell. The probe light is detected by a photodetector (PD). (b) The relevant level scheme for two-photon spectroscopy in rubidium. The coupling laser addresses either the  $|n'S_{1/2}\rangle$  or the  $|nD_{m_j}\rangle$  state(s). In (c), an example set of traces obtained for fixed probe Rabi frequency  $\Omega_p/2\pi = 191$  MHz and increasing coupling Rabi frequencies is shown. The Rydberg laser is coupled to the  $|43D_{5/2}\rangle$  state, and the number density is  $\rho_{87\text{Rb}} = (4.7 \pm 0.2) \times 10^{10} \text{ cm}^{-3}$ . Here, the oscillatory regime is preceded by an onset of bistability.

provides the coupling. However, large numbers of globally coupled oscillators with widely tunable properties are not so easily available. Therefore, a hot Rydberg vapor with  $\sim \mathcal{O}(10^9)$  atoms in the beam volume, and a somewhat lower number of oscillators, provides an ideal testbed for an experimental study of the synchronization transition for large numbers of constituent oscillators.

In our experiment, we use  $^{87}\text{Rb}$  number densities of  $\rho_{87\text{Rb}} \in [0.1, 6.1] \times 10^{11} \text{ cm}^{-3}$ , which corresponds to temperatures from  $35^\circ\text{C}$  to  $60^\circ\text{C}$  for a vapor of rubidium with natural abundance. The probe laser was locked to a detuning of  $\Delta_p/2\pi = -140$  MHz below the  $^{87}\text{Rb}$  resonance with the intermediate state  $|5S_{1/2}, F=2\rangle \rightarrow |5P_{3/2}, F=3\rangle$ . The counterpropagating coupling laser was set to scan through two-photon resonance with a  $|nS_{1/2}\rangle$  or  $|nD_{5/2}\rangle$  Rydberg state at typical scan speeds of up to  $2\pi \times 10$  MHz/ms. Typical Rabi frequencies were in the range  $\Omega_p/2\pi \in [100, 330]$  MHz and  $\Omega_c/2\pi \leq 35$  MHz for Rydberg states with principal quantum numbers  $n$  ranging from 43 to 79. Different beam waists of up to  $w \leq 1$  mm and beam waist ratios of  $w_p/w_c \approx 2, 0.9, 0.5$  have been tried, but no direct dependence on the beam waists has been observed. The data presented here were obtained for  $w_p = 390 \mu\text{m}$  and  $w_c = 440 \mu\text{m}$ . Setup and relevant level scheme are shown in Figs. 3(a) and 3(b).

Figure 3(c) shows a typical series of scans for fixed probe and increasing coupling Rabi frequency. After an onset of bistability in the optical response, a window featuring oscillations in the vapor transmission opens.

This synchronization window widens for a further increase in coupling Rabi frequency. When instead setting the coupling Rabi frequency to a fixed value, the width of the oscillation region decreases with increasing probe Rabi frequency (see also Appendix D in the Supplemental Material [41]). In the various parameter regimes that were explored experimentally, the synchronization regime is often preceded by bistability but not necessarily so. We find a strong dependence of the onset of oscillations on the Rydberg state and vapor density. Higher atom number densities require lower Rabi frequencies for the oscillations to set in. This behavior is expected from a synchronization perspective since larger global coupling strengths require lower mean-field strengths to initiate entrainment.

We observe an onset of synchronization for coupling to both  $nS$  and  $nD$  Rydberg states, though it is easier to explore the behavior and scaling when coupling to  $D$  states due to the stronger dipole coupling at similar  $n$ . The oscillations were also observed when coupling a fourth  $P$  or  $F$  state with an additional rf field in both the weak and strong driving limit, respectively. In the fully Autler-Townes split regime, oscillations occurred as long as the Rydberg population was high enough. The presence of synchronization is therefore neither a purely three-level phenomenon, nor does it depend on the orbital angular momentum of the Rydberg state.

With all system parameters held constant and fixed laser detunings, the synchronized state persists on timescales on the order of minutes, and the oscillations maintain their shape. Analysis of a time trace reveals a narrow frequency

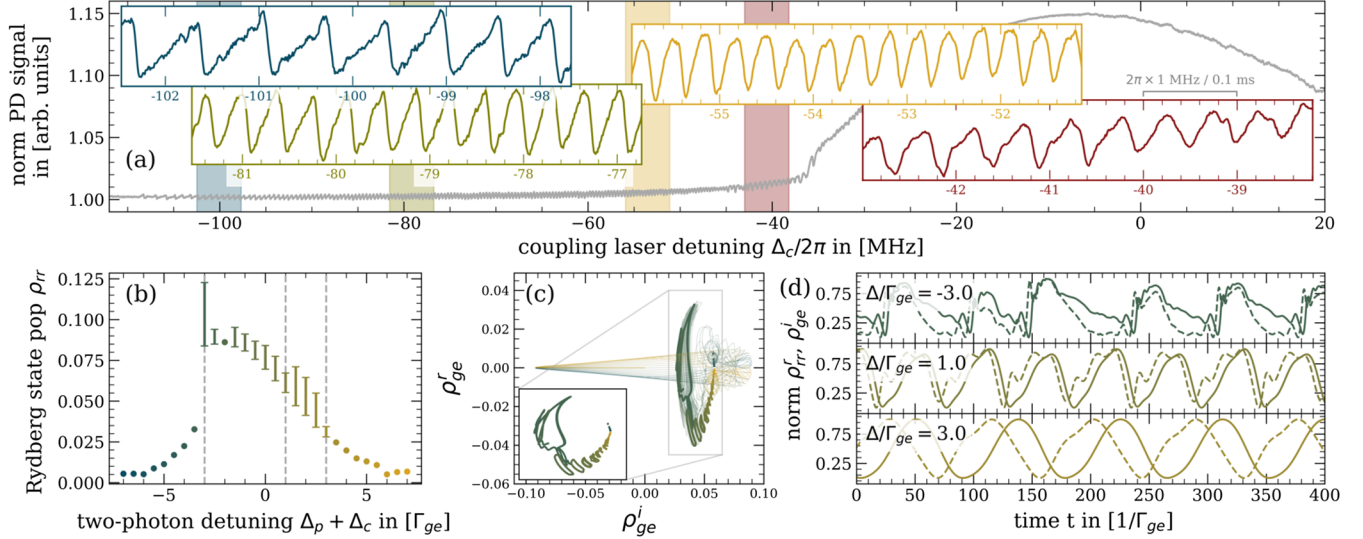


FIG. 4. Change in oscillation shape and frequency along coupling laser scan. (a) The oscillation region for a scan across resonance with  $|43D_{5/2}\rangle$  at  $T = (52.0 \pm 0.5)^\circ\text{C}$  with  $\Omega_p/2\pi = 191$  MHz,  $\Omega_c/2\pi = 37$  MHz, and a scan rate of  $2\pi \times 10$  MHz/ms. The colored insets show an enlargement of the trace in the color-shaded regions, each of width  $2\pi \times 4.8$  MHz. Different shapes of the oscillations can be distinguished. (b) Pointwise integrated spectrum with errorbars denoting the amplitude of the oscillations. The time evolution toward a limit cycle is shown in (c) with the inset showing only the limit cycles approached after an integration time of  $t = 5000\Gamma_{ge}^{-1}$ . In (d), the oscillations in Rydberg population  $\rho_{rr}^r$  (solid) and in the imaginary part of the  $c\rho_{ge}^i$  (dashed) are shown. The case  $\Delta = -3\Gamma_{ge}$  did not approach a limit cycle within the maximum integration time but behaves similar to a system near a strange attractor. The simulation assumes a thermal vapor with  $N_{\text{vel}} = 101$  velocity classes with equal populations,  $\Omega_p = 1.5$ ,  $\Omega_c = 1$ ,  $\Delta_p = 0$ ,  $\Gamma_{er} = 10^{-6}$ ,  $\Gamma_{gr} = 10^{-3}$ , and  $V = -300$ , in units of  $\Gamma_{ge}$ , and  $\beta = 2$ .

peak with a spectrum of weaker, higher harmonics (also shown in Appendix D of the Supplemental Material [41]). The oscillation frequency  $\nu_{\text{osc}}$  of the first peak was usually observed to lie between 10 kHz and 25 kHz, though persistent oscillations of up to 43 kHz were measured. In Fig. 3(c) one can see that the oscillation frequency varies along the coupling laser scan. As a general trend, an increase in oscillation frequency  $\nu_{\text{osc}}$  with increasing Rabi frequencies was observed. Additionally, the formation of several separate synchronization regions, typically with a different range  $\nu_{\text{osc}}$  but similar shapes of the oscillations along the region, has been found. This is also visible in Fig. 3(c) where the two regions share a boundary at  $-\Delta_c/2\pi \approx 26, 36, 48$  MHz for  $\Omega_c/2\pi = 29, 33, 38$  MHz, respectively.

Figure 4(a) shows the change in oscillation shape and frequency with increasing  $\Delta_c$ . Each highlighted segment samples the time dependence at a particular detuning as the laser frequency is scanned in time slowly relative to  $\nu_{\text{osc}}$ . The rightmost enlargement (red) belongs to the next synchronization region beginning at  $\Delta_c/2\pi \approx -45$  MHz. It shows again the sawtoothlike shape at its lower frequency end that can also be seen in the two leftmost insets. Figures 4(b)–4(d) show the results obtained with the thermal vapor simulation. The imaginary part of the coherence  $\rho_{ge}^i$  shown in (c) and (d, dashed) is linearly proportional to the probe laser transmission via the probe electric susceptibility [49]. Two limit cycle regions appear

in the spectrum (b), though a cross section of phase space shows that the case  $\Delta_c/\Gamma_{ge} = -3$  is not a limit cycle but resembles a system near a strange attractor. Generally, the thermal vapor model shows regions of multistability which implies that the pointwise integration technique in (b) cannot accurately model a laser scan. This is because the thermal vapor system's trajectory depends on its past state and the attractor it is drawn to, which pointwise integration does not account for.

The thermal vapor model reproduces the observed experimental behavior phenomenologically. This includes changes in the width of the synchronization region with changes in  $\Omega_p$  or  $\Omega_c$  and the earlier onset of oscillations at lower  $\Omega_c$  for increasing interaction strengths  $V$  as shown in the data of Appendix D in the Supplemental Material [41], as well as the expected shape of the oscillations. Therefore, we attribute the emergence of macroscopic oscillations in the bulk response of a hot Rydberg vapor to a Kuramoto-like synchronization transition for sufficiently large global coupling strengths. Possible mechanisms causing the power-law scaling of the Rydberg density mean field are Rydberg interactions [36] or charge-induced Stark shifts due to ionization [37], though other effects could possibly lead to similar power-law scaling behaviors.

In summary, we observe the transition toward synchronization in a strongly driven, dissipative, hot Rydberg vapor. The observed changes of the synchronized region with variation of the Rabi frequency, vapor density, and

interaction strength is reproduced by a theoretical model extended to a thermal vapor simulation. The model's nonlinearity leads to the emergence of attractive limit cycles for individual velocity classes through a Hopf bifurcation. Under the influence of global coupling through the shared Rydberg density, the constituent oscillating velocity classes synchronize in a thermal vapor, which leads to periodic oscillations of the vapor's bulk quantities. The resulting synchronized phase is robust and stable, and therefore ideally suited for an experimental investigation of the emergent nonequilibrium phase of matter. It provides a simple platform for the study of synchronization in a nonlinear system with a truly macroscopic number of oscillators.

*Note added.*—During completion of this work, two other reports of oscillations in a continuously driven hot Rydberg vapor were reported. In Ref. [50], the oscillations are of a transient nature and the probe Rabi frequency is significantly lower than in this work. The authors attribute the origin of the limit cycles to spatial inhomogeneities and clustering of Rydberg atoms. In Ref. [51], the experimental parameter regime is similar to this work. The limit cycles are attributed to a competition for Rydberg population between energetically closely spaced Rydberg states.

K. W. acknowledges insightful discussions with Finn Münnich and Matt Jamieson, and thanks Matthias Weidemüller. C. S. A. acknowledges fruitful discussions with Dong-Sheng Ding. The authors furthermore thank Lucy Downes, Max Festenstein, Oliver Hughes, and Kevin Weatherill. Financial support was provided by the UKRI, EPSRC Grant Reference No. EP/V030280/1 (“Quantum optics using Rydberg polaritons”).

\*wadenpfehl@physi.uni-heidelberg.de

†c.s.adams@durham.ac.uk

- [1] E. M. Ozbudak, M. Thattai, H. N. Lim, B. I. Shraiman, and A. van Oudenaarden, *Nature (London)* **427**, 737 (2004).
- [2] D. Angeli, J. E. Ferrell, and E. D. Sontag, *Proc. Natl. Acad. Sci. U.S.A.* **101**, 1822 (2004).
- [3] H. A. Harrington, E. Feliu, C. Wiuf, and M. P. Stumpf, *Biophys. J.* **104**, 1824 (2013).
- [4] J. P. Newman and R. J. Butera, *Chaos* **20**, 023118 (2010).
- [5] H. B. Chan, V. A. Aksyuk, R. N. Kleiman, D. J. Bishop, and F. Capasso, *Phys. Rev. Lett.* **87**, 211801 (2001).
- [6] R. L. Badzey, G. Zolfagharkhani, A. Gaidarzhly, and P. Mohanty, *Appl. Phys. Lett.* **85**, 3587 (2004).
- [7] D. N. Guerra, A. R. Bulsara, W. L. Ditto, S. Sinha, K. Murali, and P. Mohanty, *Nano Lett.* **10**, 1168 (2010).
- [8] H. M. Gibbs, S. L. McCall, and T. N. C. Venkatesan, *Phys. Rev. Lett.* **36**, 1135 (1976).
- [9] M. P. Hehlen, H. U. Güdel, Q. Shu, J. Rai, S. Rai, and S. C. Rand, *Phys. Rev. Lett.* **73**, 1103 (1994).
- [10] C. Carr, R. Ritter, C. G. Wade, C. S. Adams, and K. J. Weatherill, *Phys. Rev. Lett.* **111**, 113901 (2013).
- [11] C. G. Wade, M. Marcuzzi, E. Levi, J. M. Kondo, I. Lesanovsky, C. S. Adams, and K. J. Weatherill, *Nat. Commun.* **9**, 3567 (2018).
- [12] E. Lorenz, *J. Atmos. Sci.* **20**, 130 (1963).
- [13] M. Marek and I. Schreiber, *Chaotic Behaviour of Deterministic Dissipative Systems* (Cambridge University Press, Cambridge, England, 1991), 10.1017/cbo9780511608162.
- [14] D. Ruelle, *Elements of Differentiable Dynamics and Bifurcation Theory* (Elsevier Science & Technology Books, New York, 2014).
- [15] J. E. Marsden and M. McCracken, *The Hopf Bifurcation and Its Applications* (Springer, New York, 1976), 10.1007/978-1-4612-6374-6.
- [16] R. FitzHugh, *Biophys. J.* **1**, 445 (1961).
- [17] A. L. Hodgkin and A. F. Huxley, *J. Physiol.* **117**, 500 (1952).
- [18] T. Zhang and W. Wang, *Appl. Math. Model.* **36**, 6225 (2012).
- [19] C. Colijn and M. C. Mackey, *SIAM J. Appl. Dyn. Syst.* **6**, 378 (2007).
- [20] S. Pankavich, N. Neri, and D. Shutt, *Discrete Contin. Dyn. Syst. B* **25**, 2867 (2020).
- [21] T. E. Lee, H. Häffner, and M. C. Cross, *Phys. Rev. A* **84**, 031402(R) (2011).
- [22] K. Wiesenfeld, P. Colet, and S. H. Strogatz, *Phys. Rev. Lett.* **76**, 404 (1996).
- [23] D. Dreon, A. Baumgärtner, X. Li, S. Hertlein, T. Esslinger, and T. Donner, *Nature (London)* **608**, 494 (2022).
- [24] B. van der Pol, *London, Edinburgh, Dublin Philos. Mag. J. Sci.* **2**, 978 (1926).
- [25] Y. Kuramoto, in *International Symposium on Mathematical Problems in Theoretical Physics*, edited by H. Araki (Springer, Berlin, Heidelberg, 1975), pp. 420–422.
- [26] A. Pikovsky, M. Rosenblum, and J. Kurths, *Synchronization: A Universal Concept in Nonlinear Sciences* (Cambridge University Press, Cambridge, England, 2001).
- [27] S. H. Strogatz, *Physica (Amsterdam)* **143D**, 1 (2000).
- [28] J. A. Acebrón, L. L. Bonilla, C. J. P. Vicente, F. Ritort, and R. Spigler, *Rev. Mod. Phys.* **77**, 137 (2005).
- [29] P. Dallard, T. Fitzpatrick, A. Flint, A. Low, R. R. Smith, M. Willford, and M. Roche, *J. Bridge Eng.* **6**, 412 (2001).
- [30] I. Belykh, M. Bocian, A. R. Champneys, K. Daley, R. Jeter, J. H. G. Macdonald, and A. McRobie, *Nat. Commun.* **12**, 7223 (2021).
- [31] Y. Kuramoto, *Chemical Oscillations, Waves, and Turbulence* (Springer, Berlin, Heidelberg, 1984).
- [32] G. Ertl, *Science* **254**, 1750 (1991).
- [33] J. Buck, *Quarterly Rev. Biol.* **63**, 265 (1988).
- [34] T. J. Walker, *Science* **166**, 891 (1969).
- [35] Z. Néda, E. Ravasz, Y. Brechet, T. Vicsek, and A.-L. Barabási, *Nature (London)* **403**, 849 (2000).
- [36] N. R. de Melo, C. G. Wade, N. Šibalić, J. M. Kondo, C. S. Adams, and K. J. Weatherill, *Phys. Rev. A* **93**, 063863 (2016).
- [37] D. Weller, J. P. Shaffer, T. Pfau, R. Löw, and H. Kübler, *Phys. Rev. A* **99**, 043418 (2019).
- [38] P. Hartman, *Ordinary Differential Equations* (Society for Industrial and Applied Mathematics, Philadelphia, 2002), 10.1137/1.9780898719222.

- [39] P. Kongkhambut, J. Skulte, L. Mathey, J. G. Cosme, A. Hemmerich, and H. Keßler, *Science* **377**, 670 (2022).
- [40] T. Liu, J.-Y. Ou, K. F. MacDonald, and N. I. Zheludev, *Nat. Phys.* **19**, 986 (2023).
- [41] See Supplemental Material at <http://link.aps.org/supplemental/10.1103/PhysRevLett.131.143002> for further details on the nonlinear EOMs, the thermal vapor integrator scheme, supplemental experimental results, and comments on the continuous time crystal property. The Supplemental Material includes Refs. [37,42–44].
- [42] P. C. Parks, *Math. Proc. Cambridge Philos. Soc.* **58**, 694 (1962).
- [43] W. H. Press, S. A. Teukolsky, W. T. Vetterling, and B. P. Flannery, *Numerical Recipes 3rd Edition* (Cambridge University Press, Cambridge, England, 2007).
- [44] N. Šibalić, J. Pritchard, C. Adams, and K. Weatherill, *Comput. Phys. Commun.* **220**, 319 (2017).
- [45] A. R. Willms, P. M. Kitanov, and W. F. Langford, *R. Soc. Open Sci.* **4**, 170777 (2017).
- [46] A. T. Winfree, *J. Theor. Biol.* **16**, 15 (1967).
- [47] T. E. Lee and H. R. Sadeghpour, *Phys. Rev. Lett.* **111**, 234101 (2013).
- [48] J. Pantaleone, *Am. J. Phys.* **70**, 992 (2002).
- [49] M. Fleischhauer, A. Imamoglu, and J. P. Marangos, *Rev. Mod. Phys.* **77**, 633 (2005).
- [50] D.-S. Ding, Z. Bai, Z.-K. Liu, B.-S. Shi, G.-C. Guo, W. Li, and C. S. Adams, [arXiv:2305.07032](https://arxiv.org/abs/2305.07032).
- [51] X. Wu, Z. Wang, F. Yang, R. Gao, C. Liang, M. K. Tey, X. Li, T. Pohl, and L. You, [arXiv:2305.20070](https://arxiv.org/abs/2305.20070).